Passivating Surface Defects and Reducing Interface Recombination in $CuInS_2$ Solar Cells by a Facile Solution Treatment

*Mohit Sood, Alberto Lomuscio, Florian Werner, Aleksandra Nikolaeva, Phillip J. Dale, Michele Melchiorre, Jérôme Guillot, Daniel Abou-Ras, and Susanne Siebentritt**

Interface recombination at the absorber surface impedes the efficiency of a solar cell with an otherwise excellent absorber. The internal voltage or quasi-Fermi-level splitting (qFLs) measures the quality of the absorber. Interface recombination reduces the open-circuit voltage (V_{OC}) with respect to the qFLs. A facile solution-based sulfur postdeposition treatment (S-PDT) is explored to passivate the interface of $CuInS_2$ grown under Cu-rich conditions, which show excellent qFLs values, but much lower V_{OC}s. The absorbers are treated in S-containing solutions at 80 °C. Absolute calibrated photoluminescence and current–voltage measurements demonstrate a reduction of the deficit between qFLs and V_{OC} by almost one-third compared with the untreated device. Temperature dependence of the open-circuit voltage shows increased activation energy for the dominant recombination path, indicating less interface recombination. In addition, capacitance transients reveal the presence of slow metastable defects in the untreated solar cell. The slow response is considerably reduced by the S-PDT, suggesting passivation of these slow metastable defects. The results demonstrate the effectiveness of solution-based S-treatment in passivating defects, presenting a promising strategy to explore and reduce defect states near the interface of chalcogenide semiconductors.

1. Introduction

The copper indium gallium disulfide $Cu(In,Ga)S_2$ alloy system is a promising candidate for top cell in a thin film tandem solar cell.[1] So far, a stable efficiency of 15.5% has been achieved by growing absorber at a temperature above 550 °C.[2] $CuInS_2$, the ternary compound, allows to reduce additional effects due to alloy disorder and bandgap gradients introduced by the addition of gallium.[3–5] The $CuInS_2$ absorbers grown under Cu-excess conditions exhibit higher quasi-Fermi-level splitting (qFLs) compared with the absorbers grown under Cu-deficient conditions.[6] The qFLs represents the open-circuit voltage that the absorber itself can produce under illumination. This qFLs is still significantly lower (≈700 meV) than the bandgap (1.5 eV) of the absorber, particularly due to the presence of deep defects.[6,7] Moreover, solar cells realized with Cu-rich ([Cu]/[In], at% >1) absorbers suffer from large open–circuit voltage (V_{OC}) deficit compared with corresponding qFLs. Severe interface recombinations at the absorber/buffer (i.e., $CuInS_2$/CdS) interface are the prominent cause for this deficit.[8,9]

Interface recombination has been identified as a limiting factor in many thin film solar cells: perovskites,[10] all chalcopyrites grown under Cu excess,[11] and CdTe.[12] In that case the open-circuit voltage (V_{OC}) of the solar cell is lower than the qFLs of the absorber. Dominating interface recombination is caused by a cliff-type band offsets, i.e., conduction band minimum (CBM) of absorber is higher than CBM of buffer and/or by a high density of defects at or near the interface.[13] In Cu-rich $CuInS_2$ solar cells, both factors can play a role: an unfavorable cliff conduction band offset between $CuInS_2$/CdS and a large number of near-surface defects

M. Sood, Dr. A. Lomuscio, Dr. F. Werner, Prof. P. J. Dale, Dr. M. Melchiorre, Prof. S. Siebentritt
Department of Physics and Materials Science
University of Luxembourg
Belvaux L-4422, Luxembourg
E-mail: susanne.siebentritt@uni.lu

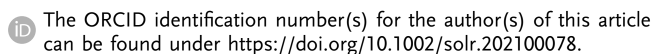
The ORCID identification number(s) for the author(s) of this article can be found under https://doi.org/10.1002/solr.202100078.

© 2021 The Authors. Solar RRL published by Wiley-VCH GmbH. This is an open access article under the terms of the Creative Commons Attribution License, which permits use, distribution and reproduction in any medium, provided the original work is properly cited.

DOI: 10.1002/solr.202100078

A. Nikolaeva, Dr. D. Abou-Ras
Department Structure and Dynamics of Energy Materials
Helmholtz-Zentrum Berlin für Materialien und Energie GmbH
Hahn-Meitner-Platz 1, 14109 Berlin, Germany

Dr. J. Guillot
Materials Research and Technology
Luxembourg Institute of Science and Technology
Belvaux L-4422, Luxembourg

in the absorber.[8,14–16] The use of an appropriate buffer layer circumvents the problem of unfavorable conduction band offset at the absorber buffer interface.[17,18] However, even with a suitable band alignment, the Cu-rich sulfide devices are still dominated by interface recombination.[19] Therefore, a suitable technique to passivate the surface defects is needed.

Recent photoluminescence (PL) studies on $CuInS_2$ and $CuInSe_2$ demonstrate that the defect chemistry in both the systems is similar, establishing a close resemblance between the two systems.[1,20] Furthermore, it has been demonstrated that both selenides and sulfide chalcopyrite solar cells are dominated by interface recombination when Cu-rich absorbers are used.[9] In a recent study, the dominating interface recombination was traced back to a defect present near the surface, which is related to a Se deficit.[21] This defect is caused by etching the $Cu_{2-x}Se$ secondary phase, which is always present in chalcopyrite grown under Cu excess.[22] This defect is responsible for the V_{OC} loss in Cu-rich solar cells. A similar defect is expected in the $CuInS_2$ compound. This defect affects the device V_{OC} in a similar way as its counterpart $CuInSe_2$. Thus, the current work aims to find a treatment that can passivate this S deficit-related defect.

In preliminary experiments, two devices were fabricated with a CdS buffer layer using low and high thiourea (CH_4N_2S) concentrations (i.e., the source of sulfur S^{2-} ions in the chemical bath solution), where the low concentration is our standard CdS recipe. The higher thiourea concentration led to a device with higher V_{OC}. As the CdS buffer layer is known to have an unfavorable band alignment with $CuInS_2$,[14,16] an additional device with Zn(O,S) buffer layer was fabricated for comparison. Details of the process for both buffer layer depositions can be found in the Supporting Information. It is worth mentioning that the concentration of thiourea in the Zn(O,S) buffer layer recipe (0.4 M) is eight times more concentrated than the standard CdS buffer layer recipe (see Supporting Information).

The current density–voltage (J–V) characteristics of the devices with different buffer layers and thiourea concentrations are shown in Figure S1, Supporting Information, which show a clear improvement in device performance, especially the V_{OC}, with the higher thiourea concentration in the chemical bath. This improvement suggests the effect of sulfur concentration on the V_{OC} of the devices. It is therefore hypothesized here that a dedicated sulfur treatment for $CuInS_2$ might be beneficial to reduce the interface recombination and improve device V_{OC}.

This study reports a sulfur postdeposition treatment (S-PDT) for Cu-rich $CuInS_2$ absorbers. For PDT, first, the secondary phase $Cu_{2-x}S$ is etched from Cu-rich absorber using 10% potassium cyanide (KCN) for 5 min followed by the S-PDT, i.e., the immersion of the absorbers in either ammonium sulfide (AS) or sodium sulfide (NaS) or thiourea (TU). Some of the absorbers were again etched with 5% KCN solution for 30 s. Finally, the absorbers are covered with buffer (Zn(O,S)) and window (aluminum-doped zinc oxide [AZO]). **Figure 1** shows the entire procedure. These solutions were chosen because they were used for surface passivation treatments on selenide absorbers in the past,[23–25] they are used in solution processing of solar cells as a part of buffer solutions,[17,26] and all of them contain sulfur species. The treatment aims at passivating surface defects related to the sulfur vacancy at or near the interface. We will demonstrate that S-PDT improves the device V_{OC} and fill factor (FF), and reduces the interface recombination, as confirmed by temperature-dependent current density–voltage–temperature (J–V–T) analysis.

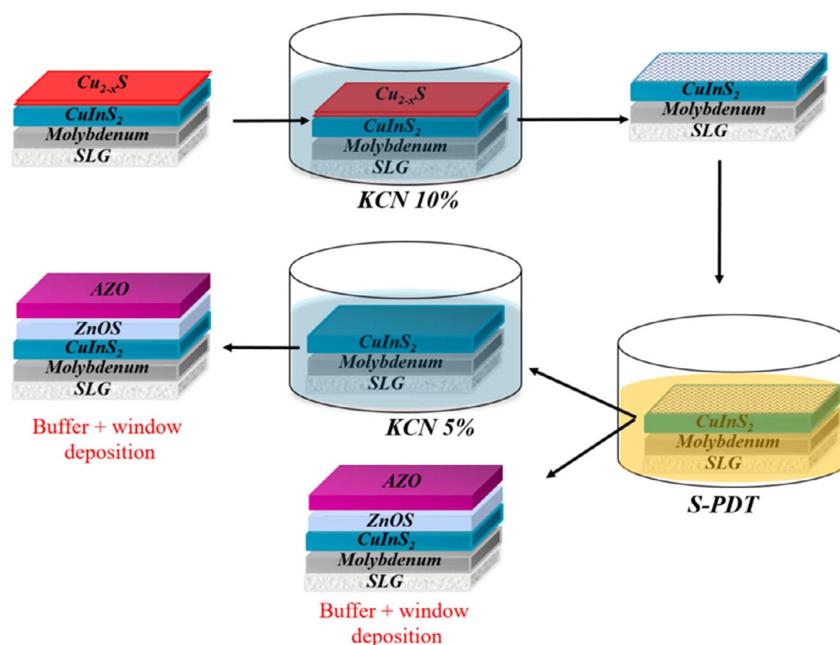

Figure 1. A schematic diagram showing the procedure used for S-PDT.

© 2021 The Authors. Solar RRL published by Wiley-VCH GmbH

2. Changes in Optoelectronic Properties with S-Treatments

2.1. QFLs Measurements

QFLs is measured by absolute calibrated PL.[27,28] **Figure 2**a shows the transformed PL spectra transformed using Planck's generalized law and the fit to extract the qFLs, measured under 5 sun illumination.[27] A bar chart of qFLs values for the untreated and S-PDT absorbers with and without a buffer layer is shown in Figure 2b. The first observation on untreated absorbers is that the buffer reduces qFLs, i.e., increases nonradiative recombination. This has been observed for all types of buffers that were tested in our lab [CdS, Zn(O,S), ZnMgO, not shown here]. As contact is necessary to make the absorber into a solar cell, it is imperative to study and improve the qFLs in absorbers covered with a buffer. Obviously, the buffer on sulfide absorbers increases recombination. This observation is in contrast to selenide absorbers, where the buffer layer was observed to passivate the surface.[28,29]

If we first compare the bare absorbers without buffers, no change in recombination activity is observed after AS-PDT, whereas NaS-PDT and TU-PDT reduce the qFLs, i.e., increase nonradiative recombination in bare absorbers. The reduction in qFLs in case of NaS-PDT is significantly more than TU-PDT. This can be a result of mechanical degradation of the absorber as during the treatment partial flaking of absorber from the Molybdenum surface was observed. However, by comparing the qFLs of absorbers with and without buffer, it becomes obvious that the NaS-PDT and TU-PDT prevent the degradation due to the buffer within measurement error. And the highest qFLs with buffer is obtained for the TU-treated absorber. The difference in recombination activity could be due to an improved interface or due to improved grain boundaries. To investigate if the S-treatment has an influence on the recombination activity of grain boundaries, the best treatment (TU-PDT) was explored by cathodoluminescence. However, no difference was observed between the cathodoluminescence of the untreated and the TU-PDT absorber (Figure S3, Supporting Information). Thus, we conclude that the main effect of the treatment is not a grain boundary passivation, but a passivation at or near the buffer/absorber interface. We investigate this further by electrical characterization of complete devices.

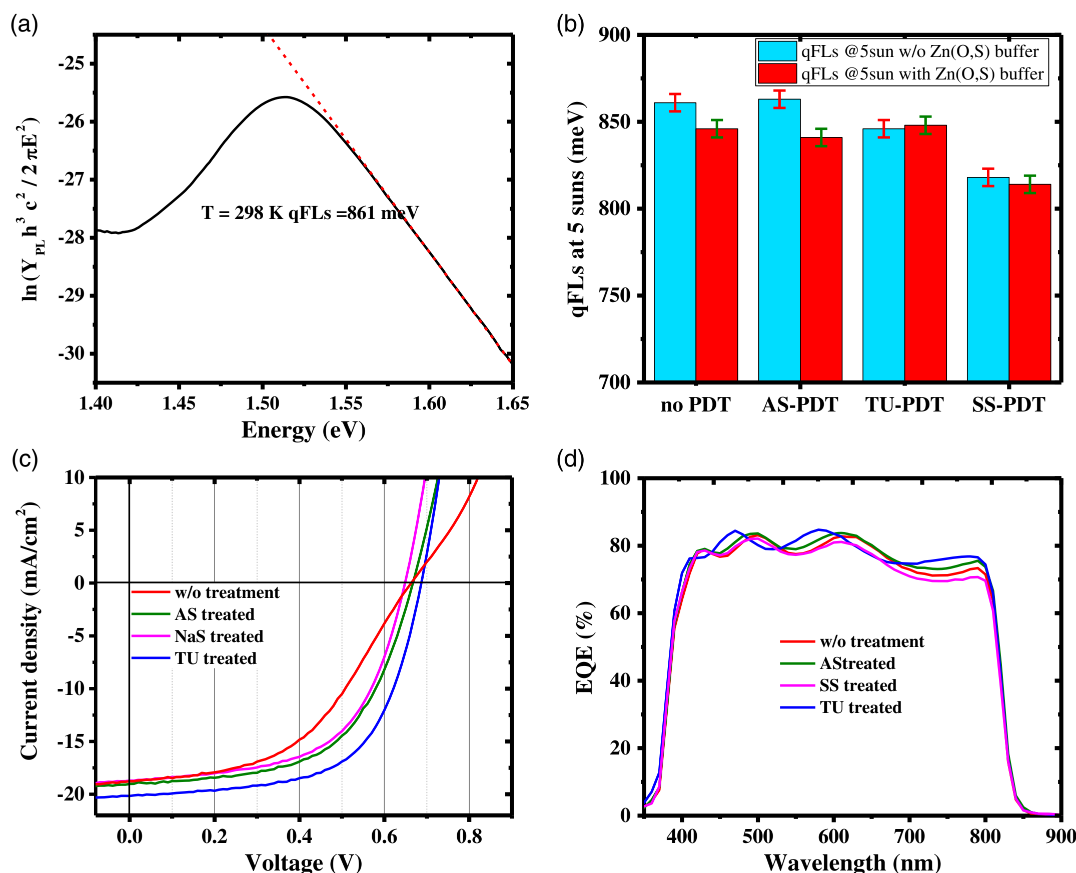

Figure 2. a) Exemplary PL spectra after approximation and transformation according to Planck's generalized law for the $CuInS_2$ device used to determine qFLs. b) QFLs values of Cu-rich $CuInS_2$ absorber treated with AS-PDT, NaS-PDT, and TU-PDT, and without any PDT under 5 sun illumination with and without Zn(O,S) buffer. c) *J–V* characteristics of Cu-rich $CuInS_2$ device with $CuInS_2$ absorber treated with AS, NaS, and TU, and reference sample without any treatment. All samples with ZnOS buffer. d) External quantum efficiencies of the $CuInS_2$ devices without any treatment and with AS-PDT, NaS-PDT, and TU-PDT.

© 2021 The Authors. Solar RRL published by Wiley-VCH GmbH

2.2. Current–Voltage Characteristics

Figure 2c shows the J–V characteristics of all treated devices together with the untreated device. The devices are as-treated, without etching after the treatment. The solar cell parameters are shown in **Table 1**, together with the shunt resistance determined from the slope of the J–V curve in reverse bias. We also list the qFLs values determined from the measurement at 5 suns on the samples with the ZnOS buffers and corrected for 1 sun illumination as explained in the Supporting Information. For the untreated device, the J–V curve exhibits an atypical "S shape" which results in a particularly low FF. The presence of defects near the surface is the origin of this "S-shaped" J–V curve, as will be discussed in the next section. Compared with the untreated device, none of the S-PDT devices exhibit the "S shape" in the J–V curves. Consequently, these devices exhibit higher FF and efficiency compared with untreated devices. The S-PDT devices also exhibit slightly improved short-circuit current density (J_{sc}) except for NaS-PDT device, which is also the one that was mechanically damaged. To better understand the short-circuit current, we study external quantum efficiency (EQE) spectra for the S-PDT and the untreated devices (Figure 2d). All devices show a lower response in the long wavelength region. It can be assumed that the space charge region (SCR) width is rather narrow, due to the high doping >1e17 cm^{-3} observed in Cu-rich $CuInS_2$ devices.[30] Obviously, the diffusion length in these devices is not long enough to compensate for the narrow SCR. As a result, there is an incomplete collection of the photons in the long wavelength region. The lowest long wavelength response is observed in the NaS-treated and potentially mechanically damaged device. In contrast, AS-PDT and TU-PDT lead to a slight improvement in the long wavelength region of the EQE spectra, suggesting improved diffusion length or SCR width after the treatment. In addition, optical effects may also play a role, as seen by the shifts in the peak wavelengths of the interference maxima. This is most evident in the EQE spectrum of the TU-PDT device, which is most distinctive among all spectra. The interference pattern in this curve is shifted to lower wavelengths (see Figure 2d). This shift in interference could be due to either a thinner buffer/window (B/W) stack compared with other devices or due to a change in the optical properties of the absorber surface due to the S-PDT. Investigation of scanning electron microscope (SEM) cross section on the devices (Figure S4, Supporting Information), however, shows very similar buffer–window thickness with an average value of 580 nm in all the devices. The differences between devices are smaller than the uncertainty of the thickness determination. This observation is expected because all the devices were processed in the same window deposition run. This eliminates the possibility of a thinner B/W in TU-treated device, and suggests the modification of the optical properties of the absorber surface, either by a modification of the surface chemistry or by deposition of an additional layer.

Among all the S-PDT devices, only the TU-PDT device shows an additional improvement in the V_{OC}, consequently exhibiting the highest PCE of 8.5%. The V_{OC} of the NaS-treated device is even lower than the one of the untreated device. In the diode model, the V_{OC} can be influenced by two main effects: the shunt resistance (R_{sh}) and the dark saturation current density (J_0) as follows[31]

$$V_{OC} = \frac{Ak_B T}{q} \times \ln\left(\frac{J_{sc}}{J_0} - \frac{V_{OC}}{J_0 R_{sh}}\right) \tag{1}$$

where q is the elementary charge, $k_B T/q$ is the thermal voltage, A is the diode factor, and J_{sc} is the photocurrent density which is assumed voltage-independent. The devices presented here have rather low shunt resistances (see Table 1); yet, the impact of R_{sh} on V_{OC} is almost negligible (see discussion in the Supporting Information). Thus, the differences in V_{OC} are due to differences in nonradiative recombination. A comparison of J_0 is not possible because the fit of the J–V characteristics to the 1-diode model is problematic, as the J–V curve does not show ideal diodic curve (more details in the Supporting Information). However, the reduction in nonradiative recombination is supported by comparing the qFLs values in Table 1 and Figure 2b: the NaS-treated sample has the lowest qFLs and the TU-treated one the highest, although not significantly higher. Still, it can be concluded from the combined observation of the trends in V_{OC} and qFLs: the nonradiative recombination in the TU-treated device is reduced.

2.3. Metastable Behavior in the Electrical Measurements

In the previous section, an "S shape" was observed in the J–V curve of the untreated device (Figure 2c). An "S shape" in the J–V curve has been observed before in chalcopyrite solar cells, particularly at lower temperatures.[32–35] The presence of this "S" shape is characteristic of a carrier transport barrier in the device and leads to the attenuation of FF and V_{OC}.[34,36–40] In the literature, the presence of a highly defective layer (p^+) at the absorber surface is invoked as an explanation: a thin layer near the surface of the absorber which has a higher net-doping than the bulk.[35,41] The formation of this p^+ layer can be

Table 1. Characteristic of best Cu-rich $CuInS_2$ device with different treatment plus reference device along with the extrapolated qFLs values at 1 sun measured on absorbers with Zn(O,S) buffer layer. The shunt resistance is determined from the inverse of the slope of the illuminated J–V curve in –0.2 to 0.0 V range. The value reported in italic font is the J_{sc} value calculated by integrating the product of EQE and AM1.5G solar spectrum, and the efficiency scaled corresponding to that of J_{sc}.

	Efficiency [%]	FF [%]	J_{sc} [mA cm^{-2}]	V_{OC} [mV]	qFLs @1 sun [meV]	qFLs − eV_{OC} [meV]	R_{sh} [ohm cm^2]
w/o treatment	6.0 (*6.8*)	48	18.8/*21.4* (EQE)	662	806	144	354
AS-PDT	7.3 (*8.4*)	57	19.0/*21.8* (EQE)	667	801	134	518
NaS-PDT	7.2 (*8.3*)	60	18.2/*21.0* (EQE)	651	771	120	373
TU-PDT	8.5 (*9.3*)	61	20.1/*21.9* (EQE)	687	808	121	456

© 2021 The Authors. Solar RRL published by Wiley-VCH GmbH

explained by the existence of the double vacancy defect (V_{Cu} and V_{Se}) in $CuInSe_2$.[42] A recent study on Cu-rich $CuInSe_2$ by Elanzeery et al. supports the model of a p^+ layer related to Se vacancies.[21] We believe a similar defect (involving V_S) might also be present in $CuInS_2$ system resulting in "S-shaped" J–V curves.

A direct consequence of this p^+ layer at the absorber surface is a conduction band bulge near the absorber buffer interface (**Figure 3**a), which originates from the leveling of the Fermi level in the system in equilibrium. This introduces an additional barrier for injected electrons under forward bias.[36,38] As a result, a voltage drop occurs across the barrier and the forward current is reduced. Moreover, defects in this p^+ layer can act as minority carrier recombination centers in the SCR under illumination.[30,43] This reduces the concentration of minority carriers near the interface. Consequently, the minority quasi-Fermi level near the interface is closer to the valence band near the surface compared with the bulk. This reduces the V_{OC} of the device to a value less than the measured qFLs by calibrated PL. Also, if the traps do not saturate under illumination, a higher hole concentration near the surface is maintained. This again leads to a conduction band bulge near the absorber, which leads to an energy barrier for the extraction of minority charge carriers (Figure 3b) and therefore to the reduction of FF and J_{sc} of the device. In addition to the p^+ layer, any barrier such as a positive conduction band offset makes the transport even worse, diminishing the FF and J_{sc} of the device even further. Therefore, in general, the "S shape" in J–V curve is more prominently visible in devices with Zn(O,S) buffer layer as compared with CdS buffer. The "S shape" and reduction of FF and J_{sc} can, in many cases, be mitigated by light soaking (LS) the device under open-circuit conditions.[33,35,36,44–50] However, placing the device in the dark for several hours can bring the device back to the initial state, i.e., with low FF and J_{sc}, indicating that the involved defects show metastable behavior.

Figure 4 shows the J–V curve of the devices that were etched after the post S-PDT along with the untreated device. In all these devices, the "S" shape is clearly observed. However, after LS for 30 min under open-circuit conditions, the "S" shape in the J–V curve disappears. The "S" shape appears again after keeping the device in the dark for 24 h (not shown here). These observations suggest $CuInS_2$ also suffers from similar metastable defects (possibly related to the Cu–S double vacancy) as in the case of $CuInSe_2$. On the contrary, in the S-PDT devices which were not subject to the second KCN etching step, the "S" shape is absent (Figure 2c and 4). These observations suggest the passivation of metastable defects, related to S-vacancies, in these devices. Still, even in these devices LS results in FF improvement (Figure 2c and Figure S6, Supporting Information), and results in a maximum device efficiency of 9.0% for the TU-PDT device (**Figure 5**a). It is worth noting that all the J–V parameters of the best device improve with LS except for V_{OC}, which is reduced. The reduction in V_{OC} is due to the degradation of the device over time, something that is commonly observed in all the devices presented in this study. This degradation can be partially recovered with LS but not completely.

To remove the S shape in J–V curve of the untreated or the etched device (Figure 4 and Figure S6, Supporting Information), a considerable duration of LS is required; this implies the engagement of "slow" defects. To explore the nature of the metastable defects in the devices, the time evolution of the SCR width of the reference device and the best S-PDT device (Figure 5b,c) was analyzed. The metastable behavior after the second KCN etch step can be seen in Figure S7, Supporting Information. The SCR width transient is measured by the inverse capacitance using the relation

$$w(t) = \varepsilon\varepsilon_0 A/C(t) \quad (2)$$

where $C(t)$ is the measured transient capacitance as follows: first, the sample is kept under illumination with a certain intensity for 300 s starting from $t = -300$ s. The "$w(t)$" is the transient SCR width of the device, ε is the relative dielectric permittivity of absorber taken equal to 10 as commonly used in the literature,[51,52] and ε_0 is the dielectric permittivity of free space. It must be noted that the measured SCR width includes contribution from both absorber and buffer. However, this fact can be ignored here as we only discuss slow metastable changes in the capacitance. Throughout this illumination period, a reverse external voltage bias is applied to make sure the device always

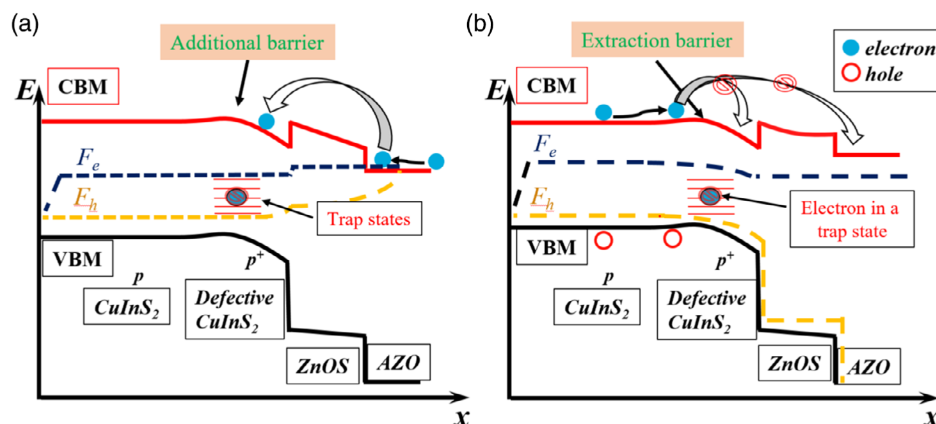

Figure 3. Band diagram sketch of $CuInS_2$ device with a p^+ layer at the absorber/buffer interface a) in the dark at moderate forward bias ≈1.0 V showing two barriers for injected electrons one at the Zn(O,S)/AZO and the other one in the p^+ layer at the front surface in the absorber b) under illumination at V_{OC} showing an extraction barrier for photogenerated minority carriers (electrons) leading to a reduced J_{sc} and FF.

© 2021 The Authors. Solar RRL published by Wiley-VCH GmbH

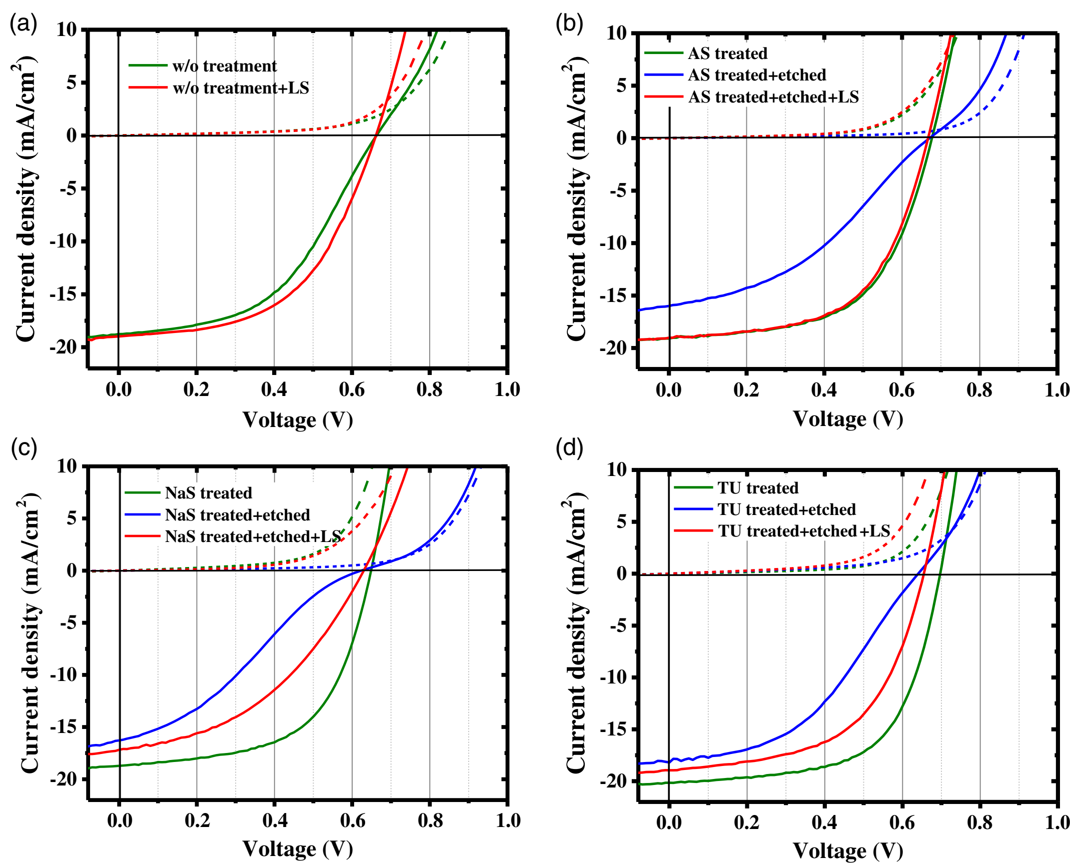

Figure 4. *J–V* curves of Cu-rich $CuInS_2$ device a) without treatment and the *J–V* curves for three different treatments with and without etching b) AS-PDT, c) NaS-PDT, and d) TU-PDT. An S shape is clearly visible in the case of the untreated and etched devices, and disappears in all devices after LS.

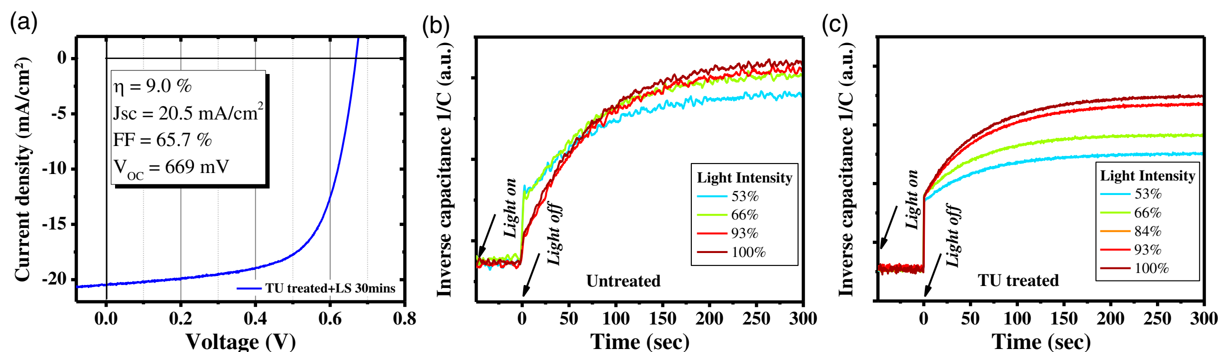

Figure 5. a) *J–V* curve of the light-soaked TU-PDT Cu-rich $CuInS_2$ device. b,c) Evolution of apparent SCR width as a function of time for different illumination levels for the untreated device and TU-treated device, respectively. The curves are shifted to have the same transient capacitance value at $t = 0$ s. The transient is measured keeping the device under illumination for 300 s before $t = 0$ s and subsequently in the dark for 300 s. The device was always kept under short-circuit condition; 100% light intensity corresponds to 1 sun intensity.

stays in short-circuit conditions (detailed information in the Supporting Information), as the internal resistance of the inductance, capacitance, and resistance LCR) meter together with the short-circuit current puts the device in forward bias state. During the illumination period, the traps are occupied with photogenerated carriers; a nearly constant capacitance toward the end of the period ensures a saturation state. The illumination intensity and the applied voltage are then set to zero at $t = 0$ s and the capacitance transient is measured for at least 300 s more. This allows the device capacitance to reach a constant value (after detrapping of carriers), indicating the device is in a new certain quasi-steady state.

Figure 5b,c shows the SCR width transients in the dark after illumination. Transients under illumination are shown in Figure S7, Supporting Information. The device capacitance is higher and thus the effective SCR width is lower under

© 2021 The Authors. Solar RRL published by Wiley-VCH GmbH

illumination due to the additional contribution of light-generated charge carriers. We are mostly interested in the SCR width change between the illuminated state and the dark state at $t = 0$ s. The device capacitance transient was measured with lowest illumination intensity first followed by higher illumination intensity. After each measurement, the device is in a quasi-steady state, which is different from the previous steady state. Bringing the device back to the completely relaxed state is extremely time-consuming. Therefore, all the curves have been shifted to the same SCR width value at $t = 0$ s to allow a better comparison; the unshifted curves can be found in the Supporting Information. For the untreated device, at $t = 0$ s, the SCR width increases abruptly (Figure 5b), as the excess of light generated carriers recombines. This fast increase in SCR width in this device decreases with the increase in illumination intensity. This is a consequence of trapping of excess charge carriers in the deep recombination centers, which release these charge carriers slowly. The gradual (slow) increase in the SCR width with time is due to the release of charge carries from the deep defects. It is interesting to note that the slow change behaves opposite to the quick jump: less slow change at lower intensities because less photogenerated carriers are trapped. The transients of the TU-PDT device (Figure 5c) show a different behavior: the abrupt change in the SCR width upon switching off light at $t = 0$ s is independent of the illumination intensity. This can be understood as a direct consequence of the passivation of the "slow" defects in the TU-PDT device. For the untreated device, these defects trap charge carriers, more so with higher illumination. After switching off the illumination, the defects release the charge carriers slowly. Under 1 sun illumination, the charge response after illumination is almost entirely given by the slow defects; there is only a very small jump in SCR width at $t = 0$ s, which can be attributed to free carriers, and almost the entire transient back to the dark state is due to slow defects. On the contrary, (partial) passivation of these defects after TU-PDT results in much less carrier trapping. The quick free-carrier response is always visible. However, the fact that the jump in SCR width remains the same and does not increase with illumination suggests that some photogenerated carriers are still trapped. The slow transient following the first jump also indicates this. The magnitude of this slow response increases with illumination, indicating more carriers trapped in slow metastable defects with higher illumination. This shows that some of these defects remain after the treatment. To complete the series, the SCR width transient measurements for the post-S-PDT KCN-etched device was also probed. Like the *J*–*V* measurements, this device shows a transient response similar to the untreated device (Figure S7c, Supporting Information), indicating the removal of the beneficial impact of TU treatment. The KCN etching is already known to preferential removal Cu and Se atoms from the Cu-rich $CuInSe_2$ lattice and thus forming ($V_{Cu} + V_S$) divacancy defect complex.[53] We hypothesize a similar mechanism also applies to Cu-rich $CuInS_2$ absorbers.

In summary, the response of the untreated device is dominated by slow defects; this response increases with higher illumination intensity, whereas the treated device shows much less response of slow defects accompanied with a free-carrier response. Thus, both *J*–*V* and capacitance transient measurements show the effectiveness of S-PDT, especially TU-PDT, in the passivation of near-surface defects. In addition, it also shows that these slow defects have characteristics, which are usually associated with metastable defects.

2.4. Interface Recombination Analysis

The low V_{OC} compared with the bandgap has been attributed to interface recombination in Cu-rich chalcopyrite solar cell.[9,21,54,55] In addition, the large deficit between the qFLs and the V_{OC} (see Table 1) is a result of recombination at or near the interface.[55,56] Temperature-dependent *J*–*V*–*T* analysis can help identify the dominant recombination pathway in the device[13]

$$J_0 = J_{00} \exp\left(\frac{-E_a}{Ak_B T}\right) \tag{3}$$

Using this together with Equation (1):

$$V_{OC} = \frac{E_a}{q} - \frac{Ak_B T}{q} \ln\left(\frac{J_{00}}{J_{sc}}\right) \tag{4}$$

where R_{sh} is ignored and J_{00} is a weakly temperature-dependent prefactor and E_a is the activation energy of the dominant recombination process. From Equation (4), a linear temperature-dependent V_{OC} extrapolation to 0 K yields the E_a of the dominant recombination process, assuming the diode factor A and the J_{sc} to be constant (at least at moderately high temperatures, i.e., 220–300 K).

Figure 6 shows the temperature dependence of the V_{OC} of the device without any treatment and devices with AS-PDT, NaS-PDT, and TU-PDT; the legend shows the activation energies. This is obtained by linear extrapolation of the high-temperature V_{OC} to 0 K. The bandgap of the devices was unaffected by treatments and was determined by the inflection point in the EQE spectra (Figure 2d). For all devices, the activation energy E_a is considerably lower than the bandgap energy E_g of the absorber. These results indicate major recombination at the absorber buffer interface in all devices. Nonetheless, the TU-PDT does

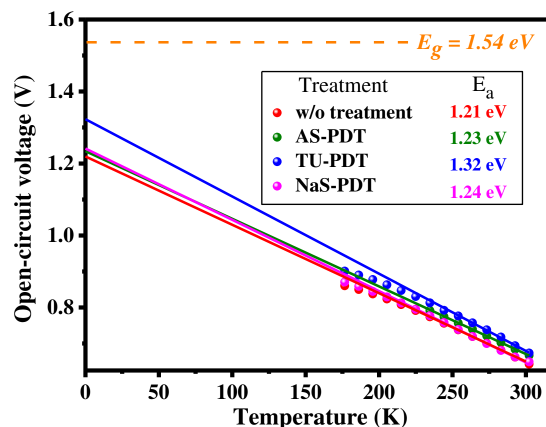

Figure 6. Open-circuit voltage versus temperature of Cu-rich $CuInS_2$ devices without any treatment, with AS-PDT, NaS-PDT, and TU-PDT. The bandgap was determined from low energy inflection point in the EQE spectrum.

© 2021 The Authors. Solar RRL published by Wiley-VCH GmbH

improve the activation energy of the devices, in agreement with the device performance trends (see Table 1). This shows a TU-PDT can particularly help reduce interface recombination in the final device.

3. Discussion: Impact of S-Salt in S-PDT

Throughout this work, the three S-PDTs have shown a different impact on device performance, with TU-PDT being the most effective among the three S-PDTs. The three S-PDTs have the same concentration of sulfur atoms in the solutions, but are different from each other with respect to the sulfur source, exact sulfur species in solution, solution pH, and the cations, as shown in **Table 2**. The PDTs AS and NaS share the same sulfur source, namely, the anion S^{2-}, whilst for TU, the origin of the sulfur is the S atom covalently bound to a carbon atom. We discuss the AS-PDTs and NaS-PDTs first. In an aqueous solution, AS ($(NH_4)_2S$) dissociates into NH_4^+ and S^{2-} and NaS (Na_2S) dissociates into Na^+ and S^{2-} ions.[57,58] We assume that the S^{2-} ion diffuses to the surface of the absorber and reacts to fill any anion vacancies. However, the exact sulfur species present in solution depends on the pH, with the more basic NaS-PDT having a higher proportion of S^{2-} ions to HS^- ions as compared with the AS-PDT.[59] The pH of the PDT solution might further impact the absorber by in-parting a different surface charge because this depends on the presence of the potential determining ion HS^-,[60] although in the subsequent solution-based deposition of Zn(O,S) this difference may be equalized again. One further detail is the presence of the cation species in the solution. The Na_2S solution contains Na^+ ions which we hypothesize that they can aggregate at grain boundaries or even go on to Cu sites in the absorber grains themselves because sodium is very mobile.[61] Both of these possibilities could have led to passivation of recombination centers and perhaps higher V_{OC} in the device. Unfortunately, though, this solution also led to delamination of the absorber from the Mo substrate during our experiments, and this accounts for the slightly degraded device performance compared with AS.

The case for TU is more complicated. Previously, it was believed that TU releases sulfur in basic conditions via HS^- to form S^{2-}.[62,63] However, a new study suggests that TU only releases sulfur when it is directly complexed to a metal cation.[64] Assuming this is correct, the TU-PDT must act differently to the AS-PDTs and NaS-PDTs. Whilst AS-PDTs and NaS-PDTs rely on the active sulfur species diffusing to the surface of the absorber layer, in the TU-PDT the CH_4N_2S molecule must diffuse and then physically adsorb first. Once adsorbed it may remain physisorbed or react with the surface of the semiconductor. If the TU physisorbs at the surface, it would lead to a thin protective layer, which may act as a physical protective barrier during the buffer layer deposition, maintaining the absorber quality. Surface X-ray photoelectron spectroscopy (XPS) analysis of the absorber treated with TU supports this argument of reaction of TU with the surface along with the presence of an additional layer linked to TU. Compared with untreated and AS-PDT absorber, XPS data of the TU-PDT absorber display the presence of a second S compound, compatible with an organic sulfur species (likely relating to TU) in addition to $CuInS_2$ (see discussion in the Supporting Information). This might explain why the qFLs does not change after depositing a buffer layer on the TU-treated absorber and at the same time provides passivation of surface defects. Furthermore, the fact that the device with TU-PDT device has different interference pattern in EQE also suggests the modification of the absorber surface.

To summarize, the different effects of the various PDTs can be due to different S-species in solution, which are expected to show different absorption behavior and reaction mechanism behavior. Further investigation of the PDTs is required to understand the reaction mechanism better. However, we would like to stress that a simple treatment with an S-containing solution does improve the interface of the solar cells.

Table 2. Summary of sulfur postdeposition treatment conditions and chemical species present in each solution.

PDT	Sulfur source	Cations	Anions	PDT pH
AS	0.4 M S^{2-}	0.8 M NH_4^+	–	9.1
NaS	0.4 M S^{2-}	2 M NH_4^+, 0.8 M Na^+	2 M OH^-	13.2
TU	0.4 M $S{=}C(NH_2)_2$	2 M NH_4^+	2 M OH^-	11.6

4. Conclusion

Interface recombination is one of the main factors for the low efficiency of Cu-rich $CuInS_2$. Using a simple sulfur solution immersion technique we were able to show partial passivation of these defects by using thiourea as a sulfur source. We probed the optoelectrical properties of Cu-rich $CuInS_2$ before and after the treatment. After buffer layer capping, the qFLs decreased in each case except for the absorber with thiourea PDT which also translated into better device performance. The current–voltage characteristics of these devices showed improved FF and efficiency with each of these treatments. However, not all the treatments were equivalent; the thiourea PDT clearly showed superior passivation ability, as indicated by the highest open-circuit voltage. On the contrary, sodium sulfide PDT did decrease the open-circuit voltage. Thus, the sulfur source in the treatment solution can also have an adverse impact and hence must be chosen carefully. The best device performance was obtained by using thiourea as the sulfur source as it improves the interface without any adverse effect on the final device properties. This was manifested in our *J–V* and *J–V–T* measurements.

In the untreated device and in devices, etched again after the S-PDT, metastabilities were observed with the help of current–voltage and slow capacitance transient measurements, and were related to a sulfur vacancy-related defect. This defect can be partially passivated by sulfur treatment, thiourea in particular, as demonstrated by our capacitance transient measurements, and can be again created at the surface by KCN etching.

The facile solution-based treatment demonstrated in this study is also applicable to other thin film solar cells, in particular chalcogenide-based ones. It can be expected that similar treatments can be developed to mitigate interface recombination and improve open-circuit voltage.

© 2021 The Authors. Solar RRL published by Wiley-VCH GmbH

5. Experimental Section

Absorber Preparation: For the experiments, two-stage absorbers were grown at 590 °C on molybdenum sputtered onto soda–lime glass (SLG) in our standard process[7] with Cu-rich elemental composition ([Cu]/[In] ≈ 1.7 and [S]/([Cu] + [In]) ≈ 0.98, as measured by energy-dispersive X-ray spectroscopy [EDX]). The two-stage process was preferred as it allowed the formation of a compact layer with a smooth surface.[7] These are important requirements to reduce shunting paths in the final device. Following the absorber growth, a 10% KCN etching for 4 min was performed to remove the $Cu_{2-x}S$ secondary phase.[65]

Postdeposition Treatment and Device Oreparation: After KCN etching, the absorbers were subjected to the sulfur treatment followed by Zn(O,S) buffer layer deposition. One absorber was not treated and directly covered with Zn(O,S) buffer layer, to have a reference device. The details for Zn(O,S) buffer layer deposition can be found in the supplementary information and are based on a recipe by Hubert et al.[66] For the S-PDT, three separate aqueous solutions consisting of $(NH_4)_2S_x$ (0.4 M), Na_2S (0.4 M) in NH_4OH (2 M) and CH_4N_2S (0.4 M) in NH_4OH (2 M), respectively, were freshly prepared in deionized (DI) water (18.2 M ohm resistivity) immediately before starting the treatment. Each of these solutions was heated to 80 °C on a hot plate. Then six freshly KCN-etched $CuInS_2$ absorbers were immersed in each of the three different solutions (two absorbers in one solution) for 10 min and afterward rinsed with DI water. After the sulfur treatment, one absorber from each treatment was again subject to 5% KCN etching for 30 s. The aim of this etching was to remove the passivating effect of the S-PDT (if any). All of these absorbers (three treated, three treated and afterward etched, and one untreated) were processed with a Zn(O,S) buffer followed by a sputtered i-ZnO (80 nm) and Al:ZnO (380 nm) window layer. Figure 1 shows the entire schematic of the previously described process. On top of the window layer, a Ni–Al dot was evaporated using an e-beam for electrical contact. Finally, the devices with SLG/Mo/$CuInS_2$/Zn(O,S)/i-ZnO/AZO architecture with an area of around 0.2 cm^2 were delineated using mechanical scribing. For qFLs measurements, one absorber from the same run was cut into small pieces. These small absorber pieces were then S-treated exactly in the same manner as the absorbers for solar cells, and then coated with Zn(O,S).

Characterization Methods: The elemental composition was measured using EDX in SEM with an operating voltage of 20 kV and for cross-sectional images operating voltage of 7 kV was used. The current–voltage (*J–V*) properties of the device were investigated using an AAA-Standard solar simulator with a Xenon short-arc lamp, calibrated by a Si reference cell, with an *I–V* source measure unit. The EQE measurements were performed using grating monochromator setup and a chopper, halogen, and xenon lamps as light source. The current is measured using a lock-in amplifier and the intensity of the light by calibrated reference diodes. Four-point admittance and temperature-dependent *J–V* measurements were performed by mounting the samples in a closed-cycle cryostat chamber, with a base pressure below 4×10^{-3} mbar. For measuring the temperature-dependent *J–V*, a cold mirror halogen lamp was used as a source for illumination. The height of the lamp from the sample was adjusted to an equivalent intensity of 100 mW cm^{-2}, by controlling for a J_{sc} equal to the one measured under the solar simulator. Precise measurement of the sample temperature was made by gluing a Si-diode sensor onto an identical glass substrate and placing it just beside the solar cell. Capacitance transients were recorded using an LCR meter with a controlled small-signal AC voltage pulse of 30 mV rms at a frequency of 10 kHz. PL measurements were conducted in a home-built system using a continuous wave 663 nm diode laser as an excitation source. For the determination of the qFLs, intensity and spectral corrections were applied to the raw data; more details can be found in these reports.[7,28]

Supporting Information

Supporting Information is available from the Wiley Online Library or from the author.

Acknowledgements

This research was funded in whole, or in part, by the Luxembourg National Research Fund (FNR), grant reference (PRIDE 15/10935404). For the purpose of open access, the author has applied a Creative Commons Attributions 4.0 International (CC BY 4.0) license to any Author Accepted Manuscript version arising from this submission. The authors also thank and acknowledge Prof. Małgorzata Igalson for her suggestions and feedback on the manuscript.

Conflict of Interest

The authors declare no conflict of interest.

Data Availability Statement

Research data are not shared.

Keywords

buffer layers, defects, interface, metastability, passivation, quasi-Fermi-level splitting, solar cells

Received: January 29, 2021
Published online: March 8, 2021

[1] M. Nakamura, K. Yamaguchi, Y. Kimoto, Y. Yasaki, T. Kato, H. Sugimoto, in *46th IEEE PVSC*, IEEE, Piscataway, NJ **2019**.
[2] T. Ott, T. Walter, D. Hariskos, O. Kiowski, R. Schäffler, *IEEE J. Photovolt.* **2012**, *3*, 514.
[3] G. E. Eperon, M. T. Hörantner, H. J. Snaith, *Nat. Rev. Chem.* **2017**, *1*, 0095.
[4] K. Yoshikawa, H. Kawasaki, W. Yoshida, T. Irie, K. Konishi, K. Nakano, T. Uto, D. Adachi, M. Kanematsu, H. Uzu, K. Yamamoto, *Nat. Energy* **2017**, *2*, 17032.
[5] T. Feurer, F. Fu, T. P. Weiss, E. Avancini, J. Löckinger, S. Buecheler, A. N. Tiwari, *Thin Solid Films* **2019**, *670*, 34.
[6] B. Tell, J. Shay, H. J. P. B. Kasper, *Phys. Rev. B* **1971**, *4*, 2463.
[7] H. Hiroi, Y. Iwata, S. Adachi, H. Sugimoto, A. Yamada, *IEEE J. Photovolt.* **2016**, *6*, 760.
[8] K. Siemer, J. Klaer, I. Luck, J. Bruns, R. Klenk, D. Bräunig, *Sol. Energy Mater. Sol. Cells.* **2001**, *67*, 159.
[9] A. Meeder, P. Schmidt-Weber, U. Hornauer, D. Förster, T. Schubert, A. Neisser, S. Merdes, R. Mainz, R. Klenk, *Thin Solid Films* **2011**, *519*, 7534.
[10] S. Merdes, R. Mainz, J. Klaer, A. Meeder, H. Rodriguez-Alvarez, H. Schock, M. C. Lux-Steiner, R. Klenk, *Sol. Energy Mater. Sol. Cells* **2011**, *95*, 864.
[11] A. Lomuscio, M. Melchiorre, S. Siebentritt, in *2018 IEEE 7th World Conf. on Photovoltaic Energy Conversion (WCPEC)*, IEEE, Piscataway, NJ **2018**, pp. 1922–1924.
[12] A. Lomuscio, T. Rödel, T. Schwarz, B. Gault, M. Melchiorre, D. Raabe, S. Siebentritt, *Phys. Rev. Appl.* **2019**, *11*, 054052.
[13] I. Hengel, A. Neisser, R. Klenk, M. C. Lux-Steiner, *Thin Solid Film.* **2000**, *361–362*, 458.
[14] M. Turcu, O. Pakma, U. Rau, *Appl. Phys. Lett.* **2002**, *80*, 2598.
[15] M. Stolterfoht, P. Caprioglio, C. M. Wolff, J. A. Márquez, J. Nordmann, S. Zhang, D. Rothhardt, U. Hörmann, Y. Amir, A. Redinger, *Energy Environ Sci.* **2019**, *12*, 2778.

© 2021 The Authors. Solar RRL published by Wiley-VCH GmbH

[16] S. Siebentritt, L. Gütay, D. Regesch, Y. Aida, V. Deprédurand, *Sol. Energy Mater. Sol. Cells* **2013**, *119*, 18.
[17] D. Kuciauskas, J. Moseley, P. Ščajev, D. Albin, *Phys. Status Solidi R* **2020**, *14*, 1900606.
[18] R. Scheer, H. Schock, *Chalcogenide Photovoltaics*, John Wiley & Sons, Wiley-VCH Verlag GmbH & Co. KGaA Weinheim **2011**, pp. 9–127.
[19] Y. Hashimoto, K. Takeuchi, K. Ito, *Appl. Phys. Lett.* **1995**, *67*, 980.
[20] B. Johnson, L. Korte, T. Lußky, J. Klaer, I. Lauermann, *J. Appl. Phys.* **2009**, *106*, 073712.
[21] L. Weinhardt, O. Fuchs, D. Groß, G. Storch, E. Umbach, N. G. Dhere, A. A. Kadam, S. S. Kulkarni, C. Heske, *Appl. Phys. Lett.* **2005**, *86*, 062109.
[22] A. Ennaoui, M. Bär, J. Klaer, T. Kropp, R. Sáez-Araoz, M. C. Lux-Steiner, *Prog. Photovolt.* **2006**, *14*, 499.
[23] M. Bär, A. Ennaoui, J. Klaer, R. Sáez-Araoz, T. Kropp, L. Weinhardt, C. Heske, H. W. Schock, C. H. Fischer, M. C. Lux-Steiner, *Chem Phys Lett.* **2006**, *433*, 71.
[24] S. Merdes, R. Sáez-Araoz, A. Ennaoui, J. Klaer, M. C. Lux-Steiner, R. Klenk, *Appl. Phys. Lett.* **2009**, *95*, 213502.
[25] A. Lomuscio, M. Sood, M. Melchiorre, S. Siebentritt, *Phys. Rev. B* **2020**, *101*, 085119.
[26] F. Babbe, H. Elanzeery, M. H. Wolter, K. Santhosh, S. Siebentritt, *J. Condens.* **2019**, *31*, 425702.
[27] H. Elanzeery, M. Melchiorre, M. Sood, F. Babbe, F. Werner, G. Brammertz, S. Siebentritt, *Phys. Rev. Mater.* **2019**, *3*, 055403.
[28] T. Gödecke, T. Haalboom, F. Ernst, *Zeitschrift für Metallkunde* **2000**, *91*, 622.
[29] D. Colombara, H. Elanzeery, N. Nicoara, D. Sharma, M. Claro, T. Schwarz, A. Koprek, M. H. Wolter, M. Melchiorre, M. Sood, N. Valle, O. Bondarchuk, F. Babbe, C. Spindler, O. Cojocaru-Miredin, D. Raabe, P. J. Dale, S. Sadewasser, S. Siebentritt, *Nat Commun.* **2020**, *11*, 3634.
[30] S. Lany, A. Zunger, *J. Appl. Phys.* **2006**, *100*, 113725.
[31] M. Igalson, M. Cwil, M. Edoff, *Thin Solid Films* **2007**, *515*, 6142.
[32] M. Turcu, U. Rau, *J. Phys. Chem. Solids* **2003**, *64*, 1591.
[33] M. Buffière, A. A. E. Mel, N. Lenaers, G. Brammertz, A. E. Zaghi, M. Meuris, J. Poortmans, *Adv. Mater.* **2015**, *5*, 1401689.
[34] M. Buffiere, T. Lepetit, S. Khelifi, A. A. El Mel, *Sol. RRL* **2017**, *1*, 1700067.
[35] S. T. Kim, L. Larina, J. H. Yun, B. Shin, B. T. Ahn, *Sustainable Energy Fuels* **2019**, *3*, 709.
[36] Y. Hashimoto, N. Kohara, T. Negami, N. Nishitani, T. Wada, *Sol. Energy Mater. Sol. Cells.* **1998**, *50*, 71.
[37] D. Regesch, L. Gütay, J. K. Larsen, V. Deprédurand, D. Tanaka, Y. Aida, S. Siebentritt, *Appl. Phys Lett.* **2012**, *101*, 112108.
[38] F. Babbe, L. Choubrac, S. Siebentritt, *Appl Phys Lett.* **2016**, *109*, 082105.
[39] J. Nelson, *The Physics of Solar Cells*, World Scientific Publishing Company, Singapore **2003**.
[40] A. Kylner, *J. Appl. Phys.* **1999**, *85*, 6858.
[41] A. Pudov, J. Sites, M. Contreras, T. Nakada, H.-W. Schock, *Thin Solid Films* **2005**, *480*, 273.
[42] A. Pudov, A. Kanevce, H. Al-Thani, J. Sites, F. Hasoon, *J. Appl. Phys.* **2005**, *97*, 064901.
[43] M. Igalson, M. Bodegård, L. Stolt, A. Jasenek, *Thin Solid Films* **2003**, *431*, 153.
[44] M. Igalson, M. Bodegård, L. Stolt, *Sol. Energy Mater. Sol. Cells* **2003**, *80*, 195.
[45] M. Igalson, C. Platzer-Björkman, *Sol. Energy Mater. Sol. Cells* **2004**, *84*, 93.
[46] M. Igalson, P. Zabierowski, D. Prządo, A. Urbaniak, M. Edoff, W. N. Shafarman, *Sol. Energy Mater. Sol. Cells* **2009**, *93*, 1290.
[47] F. Werner, M. H. Wolter, S. Siebentritt, G. Sozzi, S. Di Napoli, R. Menozzi, P. Jackson, W. Witte, R. Carron, E. Avancini, *Prog. Photovolt.* **2018**, *26*, 911.
[48] G. Sozzi, S. Di Napoli, R. Menozzi, F. Werner, S. Siebentritt, P. Jackson, W. Witte, in *2017 IEEE 44th Photovoltaic Specialist Conf. (PVSC)*, IEEE, Piscataway, NJ **2017**, pp. 2205–2208.
[49] A. Niemegeers, M. Burgelman, R. Herberholz, U. Rau, D. Hariskos, H. W. Schock, *Prog. Photovolt.* **1998**, *6*, 407.
[50] P. Jackson, D. Hariskos, R. Wuerz, O. Kiowski, A. Bauer, T. M. Friedlmeier, M. Powalla, *Phys. Status Solidi R* **2015**, *9*, 28.
[51] P. Jackson, R. Wuerz, D. Hariskos, E. Lotter, W. Witte, M. Powalla, *Phys. Status Solidi RRL* **2016**, *10*, 583.
[52] U. Rau, K. Weinert, Q. Nguyen, M. Mamor, G. Hanna, A. Jasenek, H. Schock, in *MRS Online Proc. Library Archive*, **2001**, p. 668.
[53] C. Persson, C. Platzer-Björkman, J. Malmström, T. Törndahl, M. Edoff, *Phys. Rev. Lett.* **2006**, *97*, 146403.
[54] N. Naghavi, D. Abou-Ras, N. Allsop, N. Barreau, S. Bücheler, A. Ennaoui, C. H. Fischer, C. Guillen, D. Hariskos, J. Herrero, *Prog. Photovolt.* **2010**, *18*, 411.
[55] W. Witte, D. Hariskos, A. Eicke, R. Menner, O. Kiowski, M. Powalla, *Thin Solid Films* **2013**, *535*, 180.
[56] A. Niemegeers, S. Gillis, M. Burgelman, in *Proc. of the 2nd World Conf. on Photovoltaic Energy Conversion*, JRC, European Commission,, Ispra **1998**, pp. 672–675.
[57] U. Rau, D. Braunger, H.-W. Schock, *Solid State Phenomena* **1999**, *67*, 409.
[58] F. Babbe, L. Choubrac, S. Siebentritt, *Sol. RRL* **2018**, *2*, 1800248.
[59] D. Abou-Ras, T. Kirchartz, U. Rau, *Advanced Characterization Techniques for Thin Film Solar Cells*, Wiley Online Library, Weinheim **2011**.
[60] U. Rau, A. Jasenek, H. Schock, F. Engelhardt, T. Meyer, *Thin Solid Films* **2000**, *361*, 298.
[61] V. Bessolov, E. Konenkova, M. Lebedev, *Phys. Solid State* **1997**, *39*, 54.
[62] V. N. Bessolov, E. V. Konenkova, M. V. Lebedev, *Mater. Sci. Eng. B* **1997**, *44*, 376.
[63] D. Rickard, G. W. Luther, *Chem Rev.* **2007**, *107*, 514.
[64] D. Colombara, P. J. Dale, G. P. Kissling, L. M. Peter, S. Tombolato, *J. Phys. Chem. C* **2016**, *120*, 15956.
[65] A. Laemmle, R. Wuerz, T. Schwarz, O. Cojocaru-Mirédin, P.-P. Choi, M. Powalla, *J. Appl. Phys.* **2014**, *115*, 154501.
[66] N. Pavaskar, C. Menezes, A. Sinha, *J. Electrochem. Soc.* **1977**, *124*, 743.

© 2021 The Authors. Solar RRL published by Wiley-VCH GmbH